International Journal of Scientific Research in Science, Engineering and Technology
Print ISSN: 2395-1990 | Online ISSN : 2394-4099 (www.ijsrset.com)
doi : https://doi.org/10.32628/IJSRSET1229264

Medical Image Fusion Multi Model Based on Quaternion Wavelet Transform

V. Supraja[1], K. Swetha[2], E. Haritha[3], K. Sumalatha[4], G. Chandrika[5]

[*1]Assistant Professor, Department of ECE, Ravindra college of Engineering for Women, Kurnool, Andhra Pradesh, India

[2,3,4,5]Department of ECE, Ravindra College of Engineering for Women, Kurnool, Andhra Pradesh, India

Article Info
Volume 9, Issue 2
Page Number : 348-357

Publication Issue :
March-April-2022

Article History
Accepted : 15 April 2022
Published: 30 April 2022

ABSTRACT

Medical image fusion can combine multi-modal images into an integrated higher-quality image, which can provide more comprehensive and accurate pathological information than individual image does. Traditional transform domain-based image fusion methods usually ignore the dependencies between coefficients and may lead to the inaccurate representation of source image. To improve the quality of fused image, a medical image fusion method based on the dependencies of quaternion wavelet transform coefficients is proposed. First, the source images are decomposed into low-frequency component and high-frequency component by quaternion wavelet transform. Then, a clarity evaluation index based on quaternion wavelet transform amplitude and phase is constructed and a contextual activity measure is designed. These measures are utilized to fuse the high-frequency coefficients and the choose-max fusion rule is applied to the lowfrequency components. Finally, the fused image can be obtained by inverse quaternion wavelet transform. The experimental results on some brain multi-modal medical images demonstrate that the proposed method has achieved advanced fusion result.

Keywords : Medical Image Fusion, Quaternion Wavelet Transform, Context, Activity Measure

I. INTRODUCTION

Different imaging technologies can capture different information of human body. Generally, magnetic resonance imaging (MRI) can well show normal and pathological soft tissue; however, its resolution is low and cannot reflect skeletal information. T1-magnetic resonance imaging (T1-MR) is sensitive to bleeding site and is able to provide more dissection tissue information of human body. Magnetic resonance angiography (MRA) imaging can display the structural information of narrow and closed blood vessels. Computed tomography (CT) imaging prefers to show dense tissue information,1 which mainly reflects bone and other tissue information with high resolution. Due to the variation of imaging mode, how to integrate multi-modal, images into a synthesized image is an interesting researching topic. Medical image fusion can

combine important information among multimodal images into a fused image, which provides more structure and texture and improves pathologic examination accuracy. Existing image fusion methods can be divided into two categories: the spatial domain-based fusion methods and the transform domain-based methods. The spatial domain-based image fusion method directly fuses source images at the pixel level with overlapped image blocks; this operation might lead to spatial distortion.2 The transform domain-based image fusion method usually transforms the source image into a transformed domain, in which some fusion rules are designed. With the development of multi-scale decomposition (MSD) theory, the MSD-based image fusion method has become a research hotspot. Yang3 proposed a discrete wavelet transform (DWT)-based medical image fusion algorithm, which combines wavelet coefficients according to human visual system. Yan et al.4 designed a dual-tree complex wavelet transform (DT-CWT)-based image fusion method that uses the neighborhood energy as activity measure to fuse high-frequency coefficients. He et al.5 employed contourlet transform to decompose the source images into several bands, then average fusion rule was used for low-frequency coefficients, and regional variance information was selected as activity measure for highfrequency coefficients. Zhang and Guo6 used nonsubsampled contourlet transform as a MSD tool for image fusion;the high- and low-frequency coefficients are fused by the choose-max strategy and average strategy. The traditional MSD-based image fusion methods make use of the advantages of MSD tools to some extent, but there are still some shortcomings. On the one hand, these MSD tools have their own limitations. For instance, DWT lacks phase description of image; in addition, due to the use of down-sampling operation in the decomposition process, translation invariance is absent. It may produce artifacts or false information in the fused image. CWT has only one phase angle, so it cannot solve the deviation in the vertical and horizontal directions. On the other hand, the construction of activity measurement ignores the relationship between the coefficients and fails to make full use of the feature information transmitted by decomposition coefficients. Therefore, it is necessary to make improvement in the following aspects: selecting a more superior multi-scale image decomposition tool and selecting more expressive image features Quaternion wavelet transform (QWT) is achieved by a local quaternion Fourier transform (QFT). The QFT is composed of three imaginary part and one real part7: the first two phases can describe the vertical and horizontal displacement of image features, another phase can describe the diagonal texture information of the image,8 and the amplitude has the characteristic of time-frequency localization and approximate translation invariance. In view of the superiority of QWT, many QWT-based image fusion methods have been proposed in the past few years. For example, Liu et al.9 proposed a region level-based multi-focus image fusion method using QWT that can use the local variance of the phases and structural similarity to locate the focus region. Zheng et al.10 constructed a quaternion wavelet contextual hidden Markov model to extract the statistical features for multi-focus image fusion. Thereafter, Chai et al.11 employed multiple QWT features to get fused image. This method improved the fusion quality by overcoming the inaccurate description for image caused by a single feature. The QWT-based method can produce much better fusion performance due to the better image representation from amplitude and phase of QWT. Hence, we further explore QWT-based feature extraction and apply them to fuse multi-modal medical images. To improve the representation from the texture features of QWT high-frequency coefficients, a clarity evaluation index based on the gradient of the lowfrequency amplitude, the phase of low frequency, and the phase of high frequency is proposed. Considering the dependence between QWT coefficients, a context based rule is designed for fusing the high-frequency coefficients.

The remainder of this paper is organized as follows: the next section introduces the QWT. The main framework of the proposed method and the design of fusion rules are described in the "The proposed fusion method" section. Experimental results and analyses are shown in the "Experimental results and analyses" section. Finally, we conclude this paper in the "Conclusion" section.

II. Quaternion Wavelet Transform (QWT)

In this section, we first briefly review the QWT and discuss its structure, then give a demonstration to show its capability on brain image decomposition.

Quaternion theory

I The concept of quaternion and its application in image processing were well studied.7 Suppose that there is a quaternion q, then it can be expressed as the form of q = a +bi +cj + dk, where a; b; c; and d are all real numbers. It is similar to the structure of the plural. The real part of quaternions is a; the imaginary part is the combination of the remaining three parts; and the i; j; and k in these three parts are orthogonal to each other and satisfy the following relationship.

$I^2 = j^2 = k^2 = ijk = -1, ij = k, jk = I, ik = j$ (1)

Another representation of quaternions is amplitude phase representation, which can be expressed as

$$q = |q|e^{i\phi}e^{j\theta}e^{k\Psi}, \ (\phi, \theta, \psi) \in [-\pi, \pi) \times [-\pi/2, \pi/2) \times [-\pi/4, \pi/4] \quad (2)$$

where $|q|$ is the amplitude of q, and ϕ, θ, ψ are the phase angle of q which can be obtained from the following Formula

$$\begin{cases} \phi = \arctan\left(\dfrac{2(ac+bd)}{a^2+b^2-c^2-d^2}\right) \\ \theta = \arctan\left(\dfrac{ab+cd}{a^2-b^2+c^2-d^2}\right) \\ \psi = \dfrac{1}{2}\arctan(2(ad-db)) \end{cases} \quad (3)$$

III. Two-dimensional quaternion wavelet construction

The quaternions definition of an image f(x,y) can be expressed by the following formula

$$f(x,y) = A_n^q f(x,y) + \sum_{s=1}^{n}[D_{s,1}^q, f(x,y) + D_{s,2}^q, f(x,y) + D_{s,3}^q, f(x,y)] \quad (4)$$

where $A_n^q f(x,y)$ is the approximate value of the image and $D_{s,p}^q, f(x,y)(p = 1,2,3)$ are sub-bands in three directions, respectively. The QWT of image can be achieved by the real wavelet and its 2-D Hilbert transformation

$$\begin{cases} \psi^D(x,y) = \psi_h(x)\psi_h(y) \rightarrow \psi^D + iH_{i1}\psi^D + jH_{i2}\psi^D + kH_i\psi^D \\ \psi^V(x,y) = \phi_h(x)\psi_h(y) \rightarrow \psi^V + iH_{i1}\psi^V + jH_{i2}\psi^V + kH_i\psi^V \\ \psi^H(x,y) = \psi_h(x)\phi_h(y) \rightarrow \psi^H + iH_{i1}\psi^H + jH_{i2}\psi^H + kH_i\psi^H \\ \phi(x,y) = \phi_h(x)\phi_h(y) \rightarrow \phi + iH_{i1}\phi + jH_{i2}\phi + kH_i\phi \end{cases} \quad (5)$$

where ψ^D, ψ^V, ψ^H are the wavelet functions on diagonal direction, vertical direction, and horizontal direction, respectively, and ϕ is the zoom function. The 2-D Hilbert transformation is composed of the 1-D Hilbert transformation on the x and y directions. The 2-D Hilbert transformation can be described as

$$\begin{cases} \left\{\begin{array}{c}\psi^D(x,y) = \psi_h(x)\psi_h(y) + i\psi_g(x)\psi_h(y) \\ +j\psi_h(x)\psi_g(y) + k\psi_g(x)\psi_g(y)\end{array}\right\} \\ \left\{\begin{array}{c}\psi^V(x,y) = \phi_h(x)\psi_h(y) + i\phi_g(x)\psi_h(y) \\ +j\phi_h(x)\psi_g(y) + k\phi_g(x)\psi_g(y)\end{array}\right\} \\ \left\{\begin{array}{c}\psi^H(x,y) = \psi_h(x)\phi_h(y) + i\psi_g(x)\phi_h(y) \\ +j\psi_h(x)\phi_g(y) + k\psi_g(x)\phi_g(y)\end{array}\right\} \\ \left\{\begin{array}{c}\phi(x,y) = \phi_h(x)\phi_h(y) + i\phi_g(x)\phi_h(y) \\ +j\phi_h(x)\phi_g(y) + k\phi_g(x)\phi_g(y)\end{array}\right\} \end{cases} \quad (6)$$

where $\psi^D(x,y), \psi^V(x,y), \psi^H(x,y)$ are the frequency of QWT on the direction of diagonal, vertical, and horizontal respectively, and $\phi(x,y)$ is the QWT low-frequency coefficient of image.

The following advantages of QWT transformation make it more suitable for the task of image fusion: 1.

Time-frequency localizing characteristic. Because quaternion wavelet is evolved from wavelet, it also retains the special property of wavelet timefrequency localization.

Approximate translation invariance. Because quaternion wavelet transformation uses the double tree structure in Hilbert transform pair, it has unique translation invariant characteristics compared with wavelet, shear wave, contour wave, and other decomposition tools.

Multiple coefficient information. A QWT is equivalent to four real DWTs, so at different scales, QWT can provide three phases and one amplitude of the original image.

A T1-MR brain image (Figure 1) is taken as an example to illustrate the QWT decomposition in Figure 2.

As can be seen from Figure 2, we can find that three phases of image reflect the texture structure information in vertical, horizontal, and diagonal directions. The high-frequency sub-bands of QWT mainly reflect the outline and structure information of images. In the detail region, the corresponding amplitude is relatively large. On the contrary, in the smooth region, its corresponding amplitude is relatively small.

IV. The proposed fusion method

As illustrated in Figure 3, the whole fusion process consists of four stages: decomposition with QWT

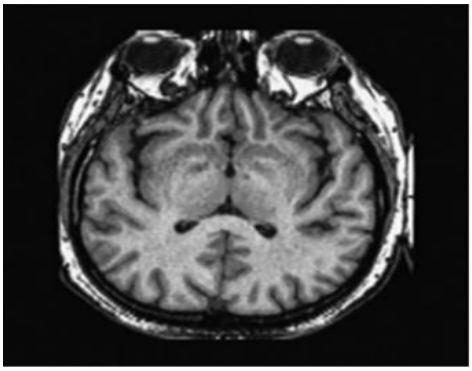

Figure 1. Brain T1-MR image.

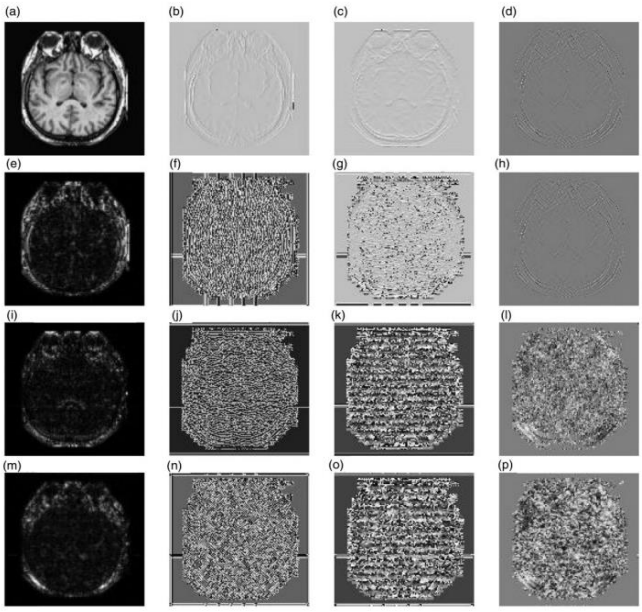

Figure 2. The QWT decomposition results of T1-MR brain image. (a) LL amplitude, (b) LL vertical phase, (c) LL horizontal phase, (d) LL diagonal phase, (e) LH amplitude, (f) LH vertical phase, (g) LH horizontal phase, (h) LH diagonal phase, (i) HL amplitude, (j) HL vertical phase, (k) HL horizontal phase, (l) HL diagonal phase, (m) HH amplitude, (n) HH vertical phase, (o) HH horizontal phase, and (p) HH diagonal phase

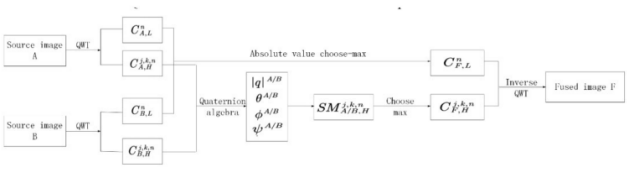

Figure 3. The framework of the proposed method. QWT: quaternion wavelet transform

fusion on low-frequency coefficients and on highfrequency coefficients, respectively, inverse transformation with QWT on fused coefficients. The detailed steps are listed as follows:

1. Decompose the pre-registered paired image A and B into low-frequency sub-bands Cn A;L; Cn B;L and highfrequency sub-bands Cj;k;n A;H; Cj;k;n B;H , where j is the decomposition scale, k is the direction,

and n represents the number of sub-bands in a direction.

2. Fuse the low-frequency coefficients with choose-max fusion rule and get the fused low-frequency coefficients.

3. Fuse the high-frequency coefficients with our proposed fusion rule and get the fused high-frequency coefficients.

4. Combine the fused low-frequency coefficients and the fused high-frequency coefficients with QWT inverse transformation and get the fused image.

The fusion rule for low-frequency sub-band coefficients The QWT low-frequency sub-band reflects the general shape of image which contains most of energy of the original image. The more prominent part can be preserved by formula (7)

$$C_{F,L}^{n}(x,y)=\begin{cases} C_{A,L}^{n}(x,y), & if|C_{A,L}^{n}(x,y)| \geq |C_{B,L}^{n}(x,y)| \\ C_{B,L}^{n}(x,y), & if|C_{A,L}^{n}(x,y)| < |C_{B,L}^{n}(x,y)| \end{cases} \quad (7)$$

where the value of n can be taken from [1,4] which presents the four sub-bands of low-frequency parts. When the absolute value of $C_{A,L}^{n}(x,y)$ is not less than $C_{B,L}^{n}(x,y)$, $C_{A,L}^{n}(x,y)$ is selected as fused coefficient $C_{F,L}^{n}(x,y)$, otherwise, $C_{B,L}^{n}(x,y)$ is taken as fused coefficient.

The fusion rule for high-frequency sub-band coefficients

Generally, the high-frequency sub-bands obtained by QWT transformation reflect the detailed texture information of image. These detail information should be transmitted as much as possible to the fused image. In this section, we introduce an amplitude and phasebased clarity evaluation index, then the highfrequency sub-bands fusion rule based on this index and the contextual relationship of coefficients.

The clarity evaluation index based on amplitude and phase. To preserve the texture details in the high-frequency sub-bands as much as possible and identify the clarityof image, a clarity metric based on phase and amplitude is proposed. First, the gradient of the amplitude of the low-frequency sub-band in the horizontal, vertical, and diagonal directions is calculated, respectively. The gradient indicates the texture change of image in three directions. The horizontal, vertical, and diagonal texture changes are measured by the horizontal phase of LH sub-band, the vertical phase of HL sub-band, and the diagonal phase of HH sub-band. For fully expressing the texture feature of image, a clarity evaluation index based on the low-frequency amplitude and three directional phase information from high frequency and low frequency is designed as follows

$$\begin{aligned} Clarity_W = \sum_{i,j\in W} & |GradL_{hor}(i,j) \times PhaseLL_{hor}(i,j) \\ & \times PhaseLH_{hor}(i,j)| + |GradL_{ver}(i,j) \\ & \times PhaseLL_{ver}(i,j) \times PhaseHL_{ver}(i,j)| \\ & + |GradL_{dia}(i,j) \times PhaseLL_{dia}(i,j) \\ & \times PhaseHH_{dia}(i,j)| \end{aligned} \quad (8)$$

where W represents an area of image with clarity value to be computed. QWT transformation is carried out to obtain the amplitude and phase information of the high- and low-frequency sub-bands. GradLhor; GradLver; GradLdia represent the gradient information of low-frequency amplitude in horizontal, vertical, and diagonal directions, respectively. PhaseLHhor; PhaseHLver; PhaseHHdia represent the phases of low-frequency coefficients in horizontal, vertical, and diagonal directions, respectively. PhaseLLhor; PhaseLLver; PhaseLLdia represent the phases information in the horizontal direction of the high-frequency LH sub-band, the vertical direction of the HL sub-band, and the diagonal direction of the HH sub-band, respectively.

The contextual activity measure of high-frequency sub-band coefficient. The MSD coefficients are related with the adjacent scale and direction.10,12 The contextual relationship of QWT coefficients is shown in Figure 5. The left part is the coarser scale, and the right part is the finer scale in three directions. Let X be the current coefficient, NA and NB are the eight nearest adjacent coefficients, PX is the parent coefficient, and CX is the cousin. X and PX, X and NA, NB, X and CX describe make the value of the activity

measure belong to (0,1). Its definition is shown as follows

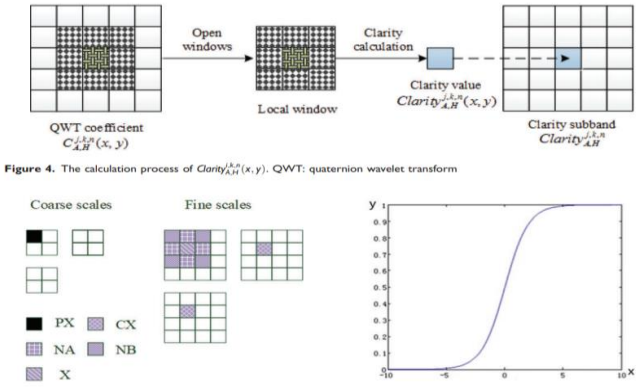

Figure 5. The context relationship schematic diagram of QWT coefficients.Figure 6. Curve graph of the erf function

$$M_{Z,H}^{j,k,n}(x,y)=\begin{cases}\left\{\begin{matrix}erf(\max_{ni,nj\in N}(Clarity_{Z,H}^{j,k,n}(x_{ni},y_{nj}) \\ -\overline{Clarity}_{Z,H}^{j,k,n})),\ j=1\end{matrix}\right\} \\ \left\{\begin{matrix}\max(erf(\max_{ni,nj\in N}(Clarity_{Z,H}^{j,k,n}(x_{ni},y_{nj}) \\ -\overline{Clarity}_{Z,H}^{j,k,n})),\ [M_{Z,H}^{j-1,k,n}]^{\downarrow 2}(x,y),j\in[2,J]\end{matrix}\right\}\end{cases} \tag{9}$$

where $Clarity_{Z,H}^{j,k,n}(x,y)$ represents the clarity feature of $C_{Z,H}^{j,k,n}(x,y)$, N is the neighborhood of the current position (x,y), and $\overline{Clarity}_{Z,H}^{j,k,n}$ represents the mean value of clarity in this neighborhood. $erf(\cdot)$ is a sigmoid-form function. The function is introduced in formula (9) to

$$erf(x)=\frac{1}{1+e^{-x}} \tag{10}$$

where x is the input variable and the curve is shown in Figure 6. The output range of erf function is (0,1), and within the range of the coefficients are monotonically increasing,down-sampling operation with a sampling factor of 2. For the high-frequency coefficient with decomposition scale of 1, the contextual activity measure is calculated directly in combination with the clarity of its neighborhood coefficient. Otherwise, the calculation of activity measure should be considered the clarity of corresponding coefficient in the previous scale. Because the size of previous scale is different with the current scale, so a down-sampling operation is necessary. Then, compare the activity measure value of current coefficient with the parent coefficient, the larger clarity value is taken as the activity measure for fusion rule. Figure 7 describes the process in detail.

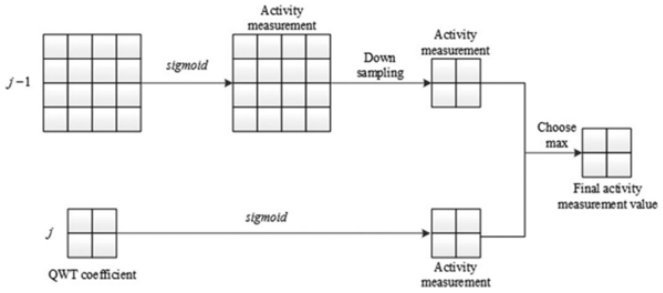

Figure 7.The calculation of active measure for high-frequency coefficient. QWT: quaternion wavelet transform.

After obtaining the activity measure of high-frequency coefficient, the fusion rule can be made as formula (11). The coefficient with the bigger activity measure value is taken as the fused high-frequency sub-band coefficient

$$C_{F,H}^{j,k,n}(x,y)=\begin{cases}C_{A,H}^{j,k,n}(x,y),\ if\ M_{A,H}^{j,k,n}(x,y)\geq M_{B,H}^{j,k,n}(x,y) \\ C_{B,H}^{j,k,n}(x,y),\ if\ M_{A,H}^{j,k,n}(x,y)<M_{B,H}^{j,k,n}(x,y)\end{cases} \tag{11}$$

V. Experimental results and analyses

In this section,The proposed fusion method is evaluated on four groups of medical images. All experiments are run on MATLAB R2015b of a PC (Pentium 3.5 GHz CPU, 8 GB RAM). Comparison of fusion methods include weighted average,13 principal component analysis,14 DWT,3 gradient pyramid transformation,15 contrast pyramid (CON),16 Q-CHMM,10 and QWT-Avg-Max.17 The parameters of the comparison method are set according to the corresponding references. In addition, the objective evaluation metrics include standard deviation, entropy, average gradient (AG), spatial frequency (SF), mutual information (MI), and edge information evaluation factor (Qabf).

A. Medical image fusion experiments on MRI–CT

Figure 8(a) and (b) shows a pair of pre-registered MRI and CT brain images. Their fusion results are shown in Figure 8(c) to (j) and the objective evaluation indexes are listed in Table 1, where the bold value indicates the best winner. As can be seen from Table 1, our proposed method wins on most metrics except on SF and MI. Figure 8(g) obtained by the CON method wins onSF metric; the reason is that the missing brightness information of MRI image leads to large grayscale variation. Figure 8(d) is almost completely similar to MRI images; few components of CT image are introduced into the fused image. Figure 8(c) and (i) loses many important detail information of the original image. Figure 8(e) and (f) loses some texture of the MRI image and results in the dark fused images. Many details of MRI image are lost in Figure 8(h). Figure 8(j) shows the fusion result of the proposed method. The fused image holds most information of the original images; the brightness and the contrast of original images are well preserved. Thus, the proposed method achieves better result in both subjective effect and objective evaluation

B. Medical image fusion experiments on the first group of T1-MR and MRA T1-MR and MRA

Images are shown in Figure 9(a) and (b). Figure 9(c) to (i) shows the fused image obtained by the comparison methods and the proposed method. Table 2 lists the objective evaluation indexes. It is obvious that Figure 9(c) has a low contrast. MI and Qabf represent the correlation between the fusion image and the original image. These two indexes get the best values because Figure 9(d) biases toward T1-MR image. Figure 9(e) preserves lots of useful information from source images, but some detail information within the T1-MR image outline is lost. In addition, Figure 9(e) to (g) is dark and has low contrast. The visual effect of Figure 9(h) is poor. Lots of detail information are lost such as the crooked outlines in the left part of the MRA image in Figure 9(i). Figure 9(j) obtained by the proposed method has the best subjective effect and optimal object indexes.

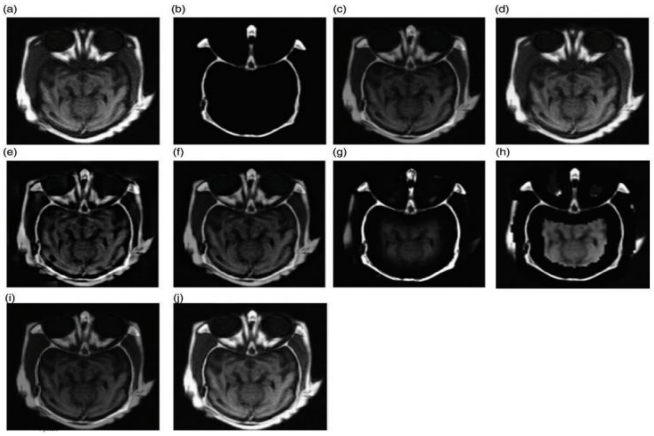

Figure 8. (a) and (b) MRI–CT medical images and their fusion results: (c) AVG, (d) PCA, (e) DWT, (f) GRA, (g) CON, (h) Q-CHMM, (i) QWT-Avg-Max, and (j) proposed.

Table 1. The objective evaluation indexes of fusion results of the MRI-CT medical image.

Fusion method	STD	EN	AG	SF	MI	Qabf
AVG	35.561	5.919	3.987	10.455	5.232	0.428
PCA	56.131	6.595	5.618	14.291	**6.323**	0.658
DWT	47.273	5.997	6.874	18.753	2.080	0.622
GRA	41.881	6.219	5.472	14.315	2.943	0.688
CON	44.578	4.679	4.858	**21.693**	2.044	0.288
Q-CHMM	46.0115	5.0656	4.9397	17.118	2.2411	0.422
QWT-Avg-Max	35.791	5.988	4.808	12.259	3.239	0.381
Proposed	**62.983**	**6.784**	**7.225**	18.102	5.054	**0.744**

C. Medical image fusion experiments on the second group of T1-MR and MRA

Figure 10(a) and (b) shows the second group T1-MR and MRA medical images, which contain more complex tissues. Their fusion results are shown in Figure 10(c) to (i) and their corresponding objective evaluation indexes are listed in Table 3. As can be seen from Figure 10, Figure 10(c) and (d) loses many texture details. Figure 10(e) is not as smooth and clear as the T1-MR image. Figure 10(f) loses some outline information of T1-MR image and the brightness

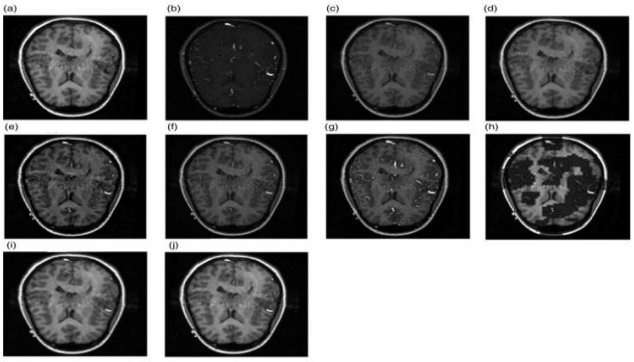

Figure 9.The fusion results of medical image (a) T1-MR and (b) MRA and the fused results based on various methods: (c) AVG, (d) PCA, (e) DWT, (f) GRA, (g) CON, (h) Q-CHMM, (i) QWT-Avg-Max, and (j) proposed information of MRA image. The outline information in Figure 10(g) is almost lost, such as the white line in the right side of the T1-MR image and the outline in the left side of MRA image. The grayscale of Figure 10(h) is unbalanced. Figure 10(i) contains some of useful information of two original images, but somedetails of MRA image are lost. Figure 10(j) preserves the outline, details, and useful features of the original images, as well as brightness and contrast, without information loss or false information. The object indexes of Figure 10(j) are consistent with subjective perception.

Table 2. The objective evaluation indexes of fusion results of the first group of T1-MR and MRA medical image.

Fusion method	STD	EN	AG	SF	MI	Qabf
AVG	45.53	5.959	6.431	16.425	5.748	0.488
PCA	57.803	6.024	7.705	20.837	**6.666**	**0.632**
DWT	54.082	5.984	10.153	**26.695**	3.054	0.548
GRA	46.623	6.307	8.6613	21.360	3.860	0.578
CON	51.185	5.727	**10.887**	26.489	3.577	0.461
Q-CHMM	58.5001	6.3295	9.9179	25.5709	3.237	0.4891
QWT-Avg-Max	67.677	6.689	9.440	23.047	3.759	0.496
Proposed	**68.209**	**6.701**	9.631	24.551	3.990	0.537

AG: average gradient; AVG: weighted average; CON: contrast pyramid; EN: entropy; GRA: gradient pyramid transformation; MI: mutual information; MRA: magnetic resonance angiography; PCA: principal component analysis; Q-CHMM: quaternion wavelet contextual hidden Markov model; QWT: quaternion wavelet transform; SF: spatial frequency; STD: standard deviation. The bold value indicates the best result.

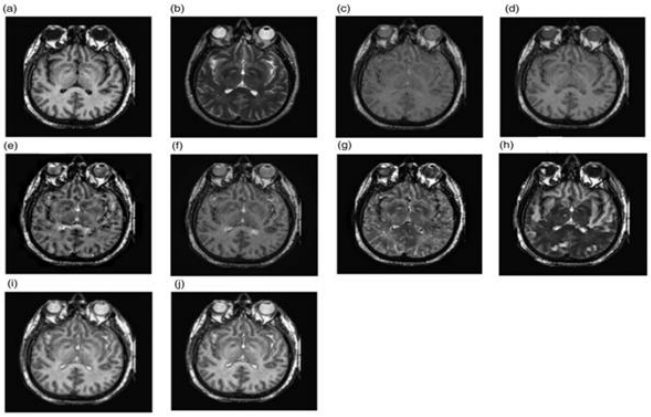

Table 3. The objective evaluation indexes of fusion results of the second group of T1-MR and MRA medical image.

Fusion method	STD	EN	AG	SF	MI	Qabf
AVG	53.77	5.329	5.863	14.976	3.769	0.357
PCA	58.933	5.587	6.753	17.273	**4.349**	0.481
DWT	62.590	6.428	**11.017**	26.650	3.267	0.464
GRA	55.292	6.471	8.312	20.308	3.477	**0.498**
CON	60.366	6.148	10.546	**27.415**	3.476	0.396
Q-CHMM	57.1379	5.8323	9.6005	23.7233	3.7026	0.4606
QWT-Avg-Max	74.122	6.095	9.229	21.874	4.006	0.439
Proposed	**74.385**	**6.501**	9.031	21.900	4.087	0.489

AG: average gradient; AVG: weighted average; CON: contrast pyramid; EN: entropy; GRA: gradient pyramid transformation; MI: mutual information; MRA: magnetic resonance angiography; PCA: principal component analysis; Q-CHMM: quaternion wavelet contextual hidden Markov model; QWT: quaternion wavelet transform; SF: spatial frequency; STD: standard deviation. The bold value indicates the best result.

Figure 10. The fusion results of the second group of (a) T1-MR and (b) MRA medical image and thefused results based on various methods: (c) AVG, (d) PCA, (e) DWT, (f) GRA, (g) CON, (h) Q-CHMM

D. Medical image fusion experiments on the third group of T1-MR and MRA

Figure 11(a) and (b) holds more complex tissue structure and texture. Their fused results are shown in Figure 11(c) to (i) and their objective evaluation indexes are listed in Table 4. Figure 11(c) seriously loses the texture details information and outline information of the original images and has low contrast, as a result, its all objective indexes are small. Figure 11(d) is excessively biased toward T1-MR images and the MI and Qabf indexes of Figure 11(d) achieve the maximum

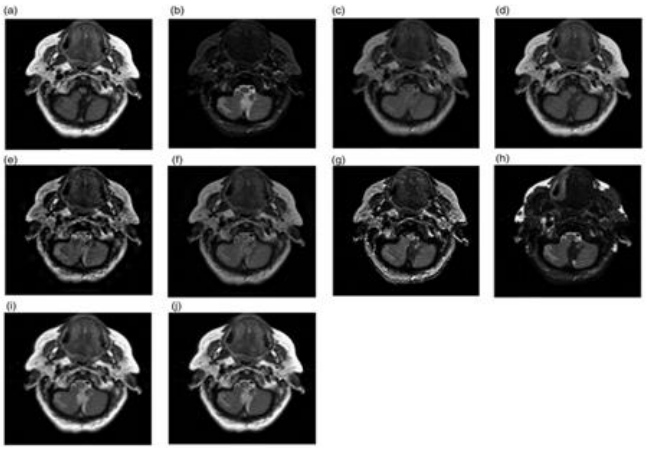

Figure 11. The fusion results of the third group of (a) T1-MR and (b) MRA medical image and the fused results based on various methods: (c) AVG, (d) PCA, (e)

DWT, (f) GRA, (g) CON, (h) Q-CHMM, (i) QWT-Avg-Max and (j) proposed values.

Table 4. The objective evaluation indexes of fusion results of the third group of T1-MR and MRA medical image.

Fusion method	STD	EN	AG	SF	MI	Qabf
AVG	47.294	5.126	5.401	13.069	3.656	0.378
PCA	61.413	5.158	6.771	17.165	**4.180**	**0.596**
DWT	55.729	5.365	9.042	22.288	2.805	0.458
GRA	48.754	5.728	7.256	17.545	3.237	0.499
CON	55.392	4.783	**11.437**	**29.520**	3.318	0.274
Q-CHMM	42.6717	4.7308	7.2114	18.4639	2.6943	0.3036
QWT-Avg-Max	72.795	5.672	8.263	19.560	3.619	0.449
Proposed	**73.079**	**5.745**	8.171	19.942	3.789	0.512

AG: average gradient; AVG: weighted average; CON: contrast pyramid; EN: entropy; GRA: gradient pyramid transformation; MI: mutual information; MRA: magnetic resonance angiography; PCA: principal component analysis; Q-CHMM: quaternion wavelet contextual hidden Markov model; QWT: quaternion wavelet transform; SF: spatial frequency; STD: standard deviation. The bold value indicates the best result.

Figure 11(e) not only has low contrast but also loses some details information, such as the two circular areas in the MRA image. Figure 11(f) is dark and blurred, and the objective evaluation indexes conform to the subjective perception. Figure 11(g) is unsmooth because of noise, which causes the AG and SF indexes win the best values. Figure 11(h) loses lots of useful information existing in source images. Figure 11(i) is blurred because it loses some small details. Due to adopting the QWT transform tool and considering the correlation between QWT coefficients, the proposed method gets the best subject perception and objective evaluation values.

VI. Conclusion

A novel medical image fusion method based on QWT has been proposed. The QWT can decompose a medical image into richer low-frequency coefficients and high-frequency coefficients. The absolute value choose-max fusion rule was adopted to fuse the lowfrequency coefficients. In addition, a clarity metric based on amplitude and phase was proposed. We have also built a novel activity measure based on the proposed clarity metric and the correlation between QWT coefficients for the high-frequency coefficients. Experimental results demonstrate that the fused medical images obtained by the proposed method preserve the important contour and texture details of the original images. Four groups of experiments on various multi-modal medical images show that the proposed method can achieve superior fusion quality in terms of both visual perception and objective evaluation.

VI. REFERENCES

[1]. Selvakumari G and Aravindh R. Directive contrast based multimodal medical image fusion with nonsubsampled contour let transform. Int J Eng Res Technol 2014; 3: 38–42.

[2]. Morris C, Rajesh R. S.. Survey of spatial domain image fusion techniques. J Adv Res Com Sc Eng and Info Tech 2014; 2: 249–254.

[3]. Yang Y. Multimodal Medical image fusion through a new DWT based technique. In: International Conferenceon Bioinformatics and Biomedical Engineering, 2010, pp.1–4. Chengdu, CN: IEEE.

[4]. Yan Y, Li L and Yang Y. Image fusion based on principal component analysis in dual-tree complex wavelet transform domain. In: International Conference on Wavelet Active Media Technology and Information Processing (ICWAMTIP), 2012, pp.70–73. Chengdu, CN: IEEE.

[5]. He Z, Zhang D, Zhang L, et al. Fusion of polarimetric image using contourlet transform. In: International Conference on Consumer Electronics, Communications and Networks (CECNet), 2011, pp.362–365. Xianning, CN: IEEE.

[6]. Zhang Q and Guo B. Research on image fusion based on the nonsubsampled contourlet transform. In: International Conference on Control and Automation, 2007, pp.3239–3243. Guangzhou, CN: IEEE.

[7]. Bayro-Corrochano E. The theory and use of the quaternion wavelet transform. J Math Imaging Vis 2006; 24: 19–35.

[8]. Gai S, Yang G and Zhang S. Multiscale texture classification using reduced quaternion wavelet transform. AEU Int J Electron Commun 2013; 67: 233–241.

[9]. Liu Y, Jin J and Wang Q. Region level based multi-focus image fusion using quaternion wavelet and normalized cut. Signal Process 2014; 97: 9–30.

[10]. Zheng X, Luo X, Zhang Z, et al. Multi-focus image fusion using quaternion wavelet transform. In: International Conference on Pattern Recognition, 2016, pp.883–888. Cancun, MX: IEEE.

[11]. Chai P, Luo X and Zhang Z. Image fusion using quaternion wavelet transform and multiple features. IEEE Access 2017; 5: 6724–6734.

[12]. Zhang H, Luo X, Wu X, et al. Statistical modeling of multi-modal medical image fusion method using C-CHMM and M-PCNN. In: International Conference on Pattern Recognition, 2014, pp.1067–1072. Stockholm, SE: IEEE.

[13]. Mumtaz A, Choi TS, Majid A, et al. Image fusion algorithm based on dual tree complex wavelet transform and support vector machine. In: International Bhurban Conference on Applied Sciences & Technology, 2010, pp. 197–202. Islamabad, PK: IEEE.

[14]. Patil U and Mudengudi U. Image fusion using hierarchical PCA. In: International Conference on Image Information Processing, 2011, pp.1–6. Shimla, IN: IEEE.

[15]. Li J, Yu J and Sun S. Study of image fusion based on grad pyramid algorithm. Sci TechnolEngI 2007; 22: 5818–5822.

[16]. Li M and Dong Y. Image fusion algorithm based on contrast pyramid and application. In: International Conference on Mechatronic Sciences, Electric Engineering and Computer, 2014, pp.1342–1345. Shengyang, CN: IEEE.

[17]. Li C, Li J and Fu B. Magnitude-phase of quaternion wavelet transform for texture representation using multilevel copula. IEEE Signal Process Lett 2013; 20: 799–802.

[18]. Xydeas CS and Petrovic V. Objective image fusion performance measure. Electron Lett 2000; 36: 308–309.

Cite this article as :

V. Supraja, K. Swetha, E. Haritha, K. Sumalatha, G. Chandrika, "Medical Image Fusion Multi Model Based on Quaternion Wavelet Transform", International Journal of Scientific Research in Science, Engineering and Technology (IJSRSET), Online ISSN : 2394-4099, Print ISSN : 2395-1990, Volume 9 Issue 2, pp. 348-357, March-April 2022. Available at doi : https://doi.org/10.32628/IJSRSET1229264
Journal URL : https://ijsrset.com/IJSRSET1229264